Direct determination of the resonance properties of metallic conical nanoantennas

Salvatore Tuccio,[1] Luca Razzari,[2,5] Alessandro Alabastri,[1] Andrea Toma,[1] Carlo Liberale,[1] Francesco De Angelis,[1] Patrizio Candeloro,[3] Gobind Das,[1] Andrea Giugni,[1] Enzo Di Fabrizio,[4,3] and Remo Proietti Zaccaria[1,6]

[1]*Nanostructures, Istituto Italiano di Tecnologia, Via Morego, 30, 16163 Genova, Italy*

[2]*Institut National de la Recherche Scientifique–Énergie Matériaux Télécommunications (INRS-EMT) 1650 Boul. Lionel-Boulet Varennes QC J3X 1S2, Canada*

[3]*University Magna Graecia, Campus S. Venuta, Germaneto, viale Europa, I88100 Catanzaro, Italy*

[4]*King Abdullah University of Science and Technology (KAUST), Physical Science and Engineering (PSE) and Biological Environmental Science and Engineering (BESE) divisions, Thuwal 23955-6900, Saudi Arabia*

[5]*e-mail: razzari@emt.inrs.ca*

[6]*e-mail: remo.proietti@iit.it*

Received September 12, 2013; revised December 16, 2013; accepted December 16, 2013; posted December 19, 2013 (Doc. ID 197508); published January 24, 2014

We present a simple method that is able to predict the resonant frequencies of a metallic conical nanoantenna. The calculation is based on an integral relation that takes into account the dependence of the effective refractive index of the plasmonic mode on the cone radius. Numerical simulations retrieving the near field properties of nanocones with different lengths are also performed for comparison. The fine agreement between the two approaches demonstrates the validity of our method. © 2014 Optical Society of America

OCIS codes: (240.6680) Surface plasmons; (310.6628) Subwavelength structures, nanostructures; (250.5460) Polymer waveguides; (250.5403) Plasmonics; (260.5740) Resonance.

http://dx.doi.org/10.1364/OL.39.000571

Optical and infrared nanoantennas have been playing a very important role in many applications such as surface-enhanced Raman spectroscopy, solar energy conversion, nanoscale microscopy, and nonlinear interactions [1]. Their success relies on the strong field enhancement generated in proximity of the structure when the resonance condition is fulfilled. A great number of investigations have been carried out in order to describe the electromagnetic properties of metal structures such as nanowires [2–5], bow-tie antennas [6], and ring-shaped disks resonators [7]. In this context, conical metallic structures have emerged as promising devices in tip-related spectroscopies, since they can efficiently guide and localize free-space radiation in a nanospot, thus promoting a stronger light–matter interaction. These remarkable features make metallic tapered structures particularly suitable as nanoprobes for scanning near-field optical microscopy (SNOM) [8], tip-enhanced Raman spectroscopy (TERS), and surface plasmon polaritons enhanced Raman scattering (SPPERS) [9], ought to their compatibility with atomic force microscopy (AFM) cantilevers [10]. Furthermore, important novel applications could be envisioned for direct infrared absorption spectroscopy. For example, in the field of protein spectroscopy in the mid-IR tips resonating around 3 μm (amide A and amide B vibration regions) or around 6 μm (amide I region) [11] can allow proper molecular identification and rich structural information. Therefore, in addition to the existing theoretical models for infinitely long conical structures [9,12] and for tapered plasmonic waveguides [13,14], a direct and reliable technique for estimating the resonance frequencies of conical nanoantennas could represent a useful tool from the near-IR to the THz regimes.

In this Letter we present a method for the determination of the electromagnetic resonances of metallic conical nanoantennas. In analogy with existing models describing cylindrical nanoantennas at optical wavelengths [15,16], a simple relation between the cone length and the resonant free-space wavelength (λ_{res}) can be derived. We stress that our approach, by employing a direct calculation of the resonance frequencies, can be extended to cones of arbitrary lengths.

An infinitely long metallic cylindrical waveguide is known to support a transverse magnetic mode (TM_0) that does not experience any cutoff even when the radius of the cylinder R is much smaller than the limit usually imposed by diffraction [17]. The complex effective refractive index $n_{\mathrm{eff}} = n_{\mathrm{eff}}^r + in_{\mathrm{eff}}^i$ associated with this mode can be derived using the following equation [18]:

$$\frac{\varepsilon_m}{\kappa_m}\frac{I_1(\gamma_m R)}{I_0(\gamma_m R)} + \frac{\varepsilon_d}{\kappa_d}\frac{K_1(\gamma_d R)}{K_0(\gamma_d R)} = 0, \tag{1}$$

where I_j and K_j ($j = 0, 1$) are the modified Bessel functions of the first and second kind, respectively, $\kappa_0 = \omega/c$, ω is the frequency of the incident radiation, c is the speed of light in vacuum, $\gamma_{m,d} = \kappa_0(n_{\mathrm{eff}}^2 - \varepsilon_{m,d})^{1/2}$, ε_m and ε_d are the permittivities associated with either the metal (m) or the surrounding dielectric (d) and $\kappa_{m,d} = \sqrt{n_{\mathrm{eff}}^2 - \varepsilon_{m,d}}$. Figure 1(a) illustrates the contour plot of the real part of the effective refractive index n_{eff}^r as a function of both radius and frequency, for a gold nanocylinder surrounded by air. The expression of the complex dielectric function of gold, described with the Drude–Lorentz model, was implemented according to [19]. The index increases monotonically by increasing the frequency at a fixed radius or by decreasing the radius at a fixed frequency. Values of n_{eff} are presented for $R \geq 5$ nm since, for smaller radii, nonlocal effects are no longer negligible and should be taken into account [20].

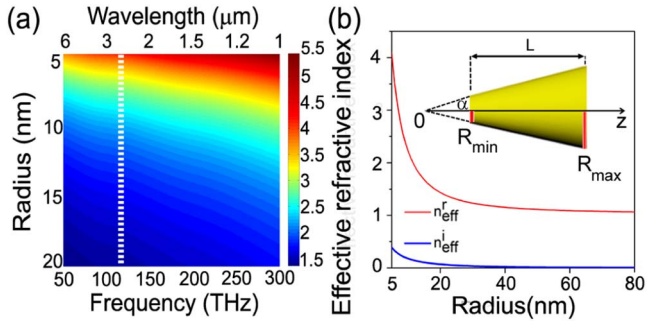

Fig. 1. (a) Contour plot of the real part of the effective refractive index of the TM_0 plasmonic mode of a gold nanocylinder, as a function of both radius and frequency. The white-dashed line marks the frequency value of 111 THz. (b) Effective refractive index [real (red) and imaginary (blue) part] as a function of radius at the dashed line ($\lambda = 2.71$ μm). Inset: sketch of the nanocone.

Starting from Eq. (1) and considering a metallic cylinder of finite length as a resonant Fabry–Perot-like cavity for the plasmonic mode, being $n^r_{\text{eff}} \gg n^i_{\text{eff}}$, the resonance condition for a cylindrical metallic antenna can be written as [16]

$$m\lambda_{\text{res}}/2 = n^r_{\text{eff}} L + 2\eta, \tag{2}$$

where m is an integer number indicating the resonance order, L is the antenna length and η accounts for the apparent increase of the antenna length originated from the phase shift acquired upon the reflections of the surface plasmon mode at the antenna ends [16].

A cone can be envisioned as a continuous sequence of coaxial cylinders with decreasing radii. Under the local mode concept, valid for slowly varying structures [21] within local domains, the plasmonic cylinder modes are good approximations to the solutions of the Maxwell's equations. Thus, for the calculation of the local effective refractive index, we can extend the use of Eq. (1) to sufficiently slowly varying geometries such as a cone with a small enough apex angle. Figure 1(b) shows the mode effective refractive index as a function of radius calculated for one specific frequency [at the dashed line of Fig. 1(a)]. By interpreting these results, we can infer that the plasmonic mode propagating over the cone surface will experience a spatially varying index, which will progressively increase during the propagation toward the tip, following the shrinkage of the cone section perpendicular to its axis. We notice that both the real (red curve) and the imaginary (blue curve) part of the index follow a similar trend, the imaginary part being much smaller than the real one.

In order to derive an expression similar to Eq. (2) for the case of a nanocone, we have to properly take into account the spatially varying effective refractive index along the structure. To do so, we have to rewrite Eq. (2) in a more general form, integrating n^r_{eff} along the z-axis from the base to the cone apex [see inset of Fig. 1(b)]. The origin of the coordinate z is set at the ideal cone apex. Since in a conical structure the radius R of the circular section of the cone at position z can be written as $R = ztg(\alpha)$, where α is the half angle at the apex, the effective index $n^r_{\text{eff}}(z)$ is in turn a function of the radius $n^r_{\text{eff}}(R)$ [13]. Therefore, by applying the concept of local modes [21], the resonant condition for the cone becomes

$$m\frac{\lambda_{\text{res}}}{2} = \frac{1}{\sin(\alpha)} \int_{R_{\min}}^{R_{\max}} n^r_{\text{eff}}(R, \lambda_{\text{res}}) dR + \eta_{R_{\min}}(\lambda_{\text{res}}) + \eta_{R_{\max}}(\lambda_{\text{res}}), \tag{3}$$

where $R_{\min} = z_{\min} \cdot tg(\alpha)$ is the minimum radius in correspondence to the physical apex and $R_{\max} = z_{\max} \cdot tg(\alpha) = (L + z_{\min}) \cdot tg(\alpha)$ is the radius at base of the cone. The terms $\eta_{R_{\max}}(\lambda_{\text{res}})$ and $\eta_{R_{\min}}(\lambda_{\text{res}})$ approximately correspond to the radial decay lengths of the mode in air (width calculated at $1/e$ of the field at the surface) at the base and at the apex of the cone, respectively. By extending a common procedure followed for cylindrical nanoantennas [15], η is taken to be equal to the corresponding section radius, therefore $\eta_{R_{\min}}$ can be neglected in Eq. (3) whenever $R_{\max} \gg R_{\min}$.

To test the validity of our method for extracting the resonance wavelengths of metallic nanocones, we have performed numerical simulations using commercial software based on a finite integration technique (CST Microwave). We have considered a gold conical structure embedded in air, with a base radius $R_{\max} = 100$ nm, tip radius of curvature $R_{\min} = 5$ nm and variable lengths (from 600 nm to 2 μm). The complex dielectric function of gold was again taken from [19]. The cone is illuminated by either a plane wave (PW) polarized along the axis of the cone or by an axial symmetric radial source (RS) positioned below its basis. The considered excitation methods generate in the device both the HE_1-like-mode and the TM_0 mode (PW) [22] or a pure TM_0 mode (RS). However, considering that the HE_1-like-mode undergoes a cutoff with radius shrinkage, only the TM_0 will be present at the tip apex, being thus the sole mode able to resonate. Figure 2 shows the near field enhancement F_{PW} and F_{RS} [defined as the ratio between the field at the apex of the cone and the free-space incoming field (PW), or the field calculated at the base of the cone (RS)] as a function of frequency, for cones with six different lengths and fixed base radius ($R_{\max} = 100$ nm). As expected,

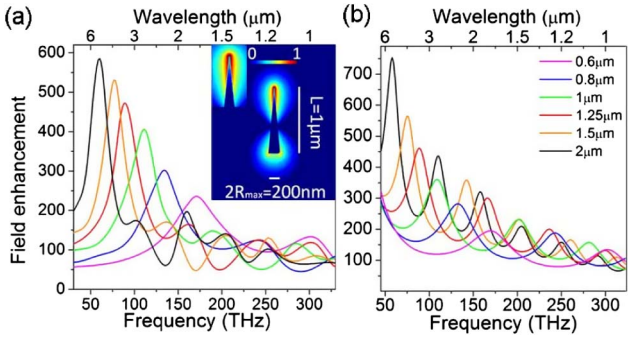

Fig. 2. F as a function of frequency for different cone lengths. (a) PW case. Inset: normalized electric field (log-scale plot) around the nanocone ($L = 1$ μm, $R_{\max} = 100$ nm) at the resonance condition ($\lambda = 2.71$ μm, dashed line position of Fig. 1). (b) RS case. To be noticed that, both excitations are able to drive TM_0 even and odd resonances.

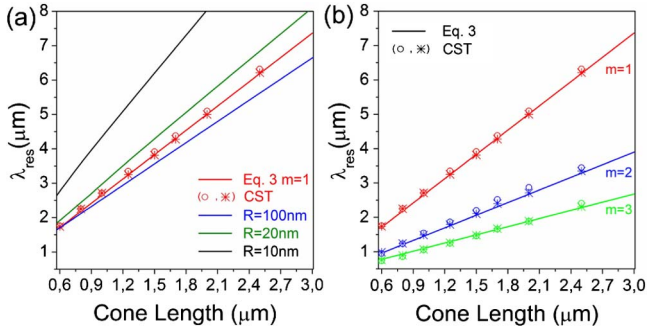

Fig. 3. (a) Fundamental resonant wavelength λ_{res} as a function of the cone length L ($R_{max} = 100$ nm). Red line: calculated using Eq. 3 ($m = 1$); Scatter symbols: CST simulations (circle, plane wave; asterisk, radial source). The relation between λ_{res} and L is also shown for Au cylinders having three different radii. (b) λ_{res} versus L for the first three resonance orders ($m = 1, 2, 3$).

both excitations determine a similar optical response from the structure. For all the considered lengths, a clear first-order resonance is observed, covering the mid-IR region from about 1.7 to 6 μm. This main peak is then followed by some lower peaks, ascribable to higher-order resonant modes. By increasing L, both a red-shift of the first-order resonance and an increase of the field enhancement value at resonance can be observed. Figure 2(a) (inset) also shows the normalized total electric field around the structure under resonant conditions, together with a zoom of the tip region (the cone dimensions are $L = 1$ μm and $R_{max} = 100$ nm, in this case). The field is found to be highly localized in proximity of the apex and the field distribution around the structure takes the expected dipolar shape.

To compare the developed method with the results of the numerical simulations, Eq. (3) has been numerically implemented (trapezoidal integration technique) and the result of the calculation is presented in Fig. 3 (red lines). In Fig. 3(a), we have focused our attention on the first-order resonance of the cone [$m = 1$ in Eq. (3)] since it is the one that produces the highest near field enhancement and is thus the most interesting for practical applications. We notice a fine agreement between the resonance positions obtained with the developed method and the ones extracted from the simulations in Fig. 2 (circles and asterisks in Fig. 3).

Furthermore, Fig. 3(a) also shows the relation between λ_{res} and L for Au cylinders having radius from 10 to 100 nm (the latter is the base of the simulated cone). The results strongly indicate the necessity of a radius adaptive expression such as Eq. (3) in order to properly describe the resonance wavelength of a metallic cone.

Finally, Fig. 3(b) shows the results obtained with the proposed model when the first three resonance orders ($m = 1, 2, 3$) are considered. Once again, a good agreement with the results of the simulations is found.

In conclusion, we have developed a direct method that exactly provides the spectral position of the resonances of a metallic nanocone of finite length and we have demonstrated its validity through the comparison with the results of numerical simulations. We have limited our investigation to the first three resonant modes of nanocones resonating at mid-infrared wavelengths. The method can be straightforwardly applied to higher-order resonance modes and in a wider spectral range (spanning from the near-IR to the THz region). This study might find interesting and valuable applications in several research fields, contributing, for example, to the improvement of spectroscopic techniques such as surface-enhanced infrared absorption by means of a single 3D nanoantenna fully compatible with AFM spectroscopy, as well as opening novel perspectives in nonlinear optical investigations of single nano-objects properly positioned in proximity of the nanocone apex.

The authors gratefully acknowledge support from the European project FOCUS FP7 no. 270483. L. R. also acknowledges financial support from NSERC Discovery Grant and FQRNT Nouveaux Chercheurs Grant.

References

1. P. Biagioni, J. S. Huang, and B. Hecht, Rep. Prog. Phys. **75**, 2941 (2012).
2. F. Neubrech, D. Weber, J. Katzmann, C. Huck, A. Toma, E. Di Fabrizio, A. Pucci, and T. Härtling, ACS Nano **6**, 7326 (2012).
3. G. W. Bryant, F. J. Garcia de Abajo, and J. Aizpurua, Nano Lett. **8**, 631 (2008).
4. L. Razzari, A. Toma, M. Shalaby, M. Clerici, R. Proietti Zaccaria, C. Liberale, S. Marras, I. A. I. Al-Naib, G. Das, F. De Angelis, M. Peccianti, A. Falqui, T. Ozaki, R. Morandotti, and E. Di Fabrizio, Opt. Express **19**, 26088 (2011).
5. C. D'Andrea, J. Bochterle, A. Toma, C. Huck, F. Neubrech, E. Messina, B. Fazio, O. M. Maragò, E. Di Fabrizio, M. Lamy de La Chapelle, P. G. Gucciardi, and A. Pucci, ACS Nano **7**, 3522 (2013).
6. H. Fischer and O. J. F. Martin, Opt. Express **16**, 9144 (2008).
7. Y. Gu, Q. Li, and G. P. Wang, Opt. Lett. **36**, 3326 (2011).
8. S. Palomba and L. Novotny, Nano Lett. **9**, 3801 (2009).
9. R. Proietti Zaccaria, A. Alabastri, F. De Angelis, G. Das, C. Liberale, A. Toma, A. Giugni, L. Razzari, M. Malerba, H. B. Sun, and E. Di Fabrizio, Phys. Rev. B **86**, 035410 (2012).
10. F. De Angelis, G. Das, P. Candeloro, M. Patrini, M. Galli, A. Bek, M. Lazzarino, I. Maksymov, C. Liberale, L. C. Andreani, and E. Di Fabrizio, Nat. Nanotechnol. **5**, 67 (2009).
11. F. Huth, A. Chuvilin, M. Schnell, I. Amenabar, R. Krutokhvostov, S. Lopatin, and R. Hillenbrand, Nano Lett. **13**, 1065 (2013).
12. A. J. Babadjanyan, N. L. Margaryan, and A. K. V. Nerkararyan, J. Appl. Phys. **87**, 3785 (2000).
13. M. Stockman, Phys. Rev. Lett. **93**, 137404 (2004).
14. A. Alabastri, A. Toma, C. Liberale, M. Chirumamilla, A. Giugni, F. De Angelis, G. Das, E. Di Fabrizio, and R. Proietti Zaccaria, Opt. Express **21**, 7538 (2013).
15. L. Novotny, Phys. Rev. Lett. **98**, 266802 (2007).
16. E. Cubukcu and A. F. Capasso, Appl. Phys. Lett. **95**, 201101 (2009).
17. L. Novotny and C. Hafner, Phys. Rev. E **50**, 4094 (1994).
18. D. Sarid and W. Challener, *Modern Introduction to Surface Plasmons* (Cambridge, 2010).
19. A. D. Rakic, A. B. Djuricic, J. M. Elazar, and M. L. Majewski, Appl. Opt. **37**, 5271 (1998).
20. A. Wiener, A. I. Fernandez-Dominguez, A. P. Horsfield, J. B. Pendry, and S. A. Maier, Nano Lett. **12**, 3308 (2012).
21. A. W. Snyder and J. D. Love, *Optical Waveguide Theory* (Springer, 1983).
22. R. Proietti Zaccaria, F. De Angelis, A. Toma, L. Razzari, A. Alabastri, G. Das, C. Liberale, and E. Di Fabrizio, Opt. Lett. **37**, 545 (2012).